

Ab initio theory of N_2V defect as quantum memory in diamond

Péter Udvarhelyi,^{1,2} Gergő Thiering,^{2,3} Elisa Londero,² and Adam Gali^{2,3}

¹Loránd Eötvös University, Pázmány Péter sétány 1/A, H-1117 Budapest, Hungary

²Institute for Solid State Physics and Optics, Wigner Research Centre for Physics, Budapest, Hungary

³Budapest University of Technology and Economics, Budafoki út 8., H-1111 Budapest, Hungary

(Dated: April 25, 2017)

N_2V defect in diamond is characterized by means of *ab initio* methods relying on density functional theory calculated parameters of a Hubbard model Hamiltonian. It is shown that this approach appropriately describes the energy levels of correlated excited states induced by this defect. By determining its critical magneto-optical parameters, we propose to realize a long-living quantum memory by N_2V defect in diamond.

Paramagnetic point defects in diamond are candidates for quantum bit and quantum information applications. Various defects were identified as optically active color centers[1], most notable is the nitrogen-vacancy (NV)[2]. NV is formed in diamond by trapping of a mobile vacancy by the substitutional nitrogen atom. In nitrogen rich diamond aggregation of substitutional nitrogen atoms may occur. The neighbor substitutional nitrogen pair is an example for such aggregation (A-aggregate). Similar to NV defect, N_2V defect is formed by an A-aggregate trapping a mobile vacancy[3]. Uniaxial stress measurements already established N-V-N structure of the N_2V defect with C_{2v} symmetry [see Fig. 1(a)] [4]. The effective one-electron picture of the defect is described by Lowther[5]. The defect in its neutral charge state was assigned to H3 color center[6] with zero phonon line (ZPL) of 2.463 eV, where this signal was associated with the optical transition between 1A_1 ground and 1B_1 excited state[7]. The H3 photoluminescence (PL) center has a PL lifetime of 17.5 ns and outstanding 0.95 quantum yield[8] that makes the defect a stable single photon source[9]. An optically inactive 1A_1 state with absorption line at 2.479 eV was revealed under uniaxial stress measurements[7]. Furthermore, H13 absorption band with ZPL at 3.364 eV was also observed and interpreted as transition to higher excited states[10]. The H3 center shows delayed luminescence, that was interpreted as a reversible transition from the 1B_1 excited state to metastable triplet states, with radiative decay time in the order of tens of milliseconds[11]. Its paramagnetic metastable triplet state was investigated by electron spin resonance (ESR) spectroscopy, called W26 center, under illumination at room temperature. The experimental zero-field splitting (ZFS) tensor principal values are $D_{xx} = 1.43$ GHz and $D_{zz} = -2.63$ GHz. The measured hyperfine parameters of ^{14}N nuclei are $A_{\perp} = 10.2$ MHz and $A_{\parallel} = 21.5$ MHz[12].

Our study is motivated by the success of optically detected magnetic resonance (ODMR) applications of single NV defect[13] and the readout and control of single nuclear spin with ST1 defect in diamond[14]. The latter employs optical pumping to metastable triplet state

where initialization of the nuclear spin is achieved by spin polarization transfer exploiting the hyperfine level anti-crossing (LAC). As the metastable triplet state relaxes to the singlet ground state, the nuclear spin coherence time is not reduced by the persistent electron spin. As H3 center exhibits singlet ground state and optically accessible metastable triplet state we wished to explore the properties of N_2V defect for quantum memory applications.

To this end, we characterize this defect in diamond by means of advanced density functional theory (DFT) calculations. In this paper, we demonstrate that optical spin polarization of the triplet state and spin polarization transfer to the existing nuclear spins is principally feasible, i.e., a long living quantum memory may be realized with N_2V defect. Their magneto optical parameters is determined by means of DFT calculations that go beyond the conventional Kohn-Sham DFT methods. By novel combination of von Barth theory[15] and Hubbard model we developed an *ab initio* method to calculate the energy of highly correlated multiplets with using only Kohn-Sham DFT wavefunction and energies, and we apply this to the neutral N_2V defect.

We carried out DFT calculations for electronic structure calculation and geometry optimization within HSE06 hybrid functional[16] using the plane wave based Vienna Ab initio Simulation Package (VASP)[17–20]. The core electrons were treated in the projector augmented-wave (PAW) formalism[21]. The model of N_2V in bulk diamond was constructed using a 512-atom diamond simple cubic supercell within the Γ -point approximation. The calculations were performed with 370 eV plane wave cutoff energy. Hyperfine interaction parameters were obtained with core correction included[22] with an increased cutoff energy of 500 eV. Zero field splitting parameters were calculated with a home built code[23]. HSE06 calculations provided excellent results for N_2V^- defect (see Ref. 24) but we found that the neutral N_2V is very challenging for Kohn-Sham DFT functional because of the highly correlated open-shell orbitals. We present our novel method to properly calculate these states that involves a Hubbard model

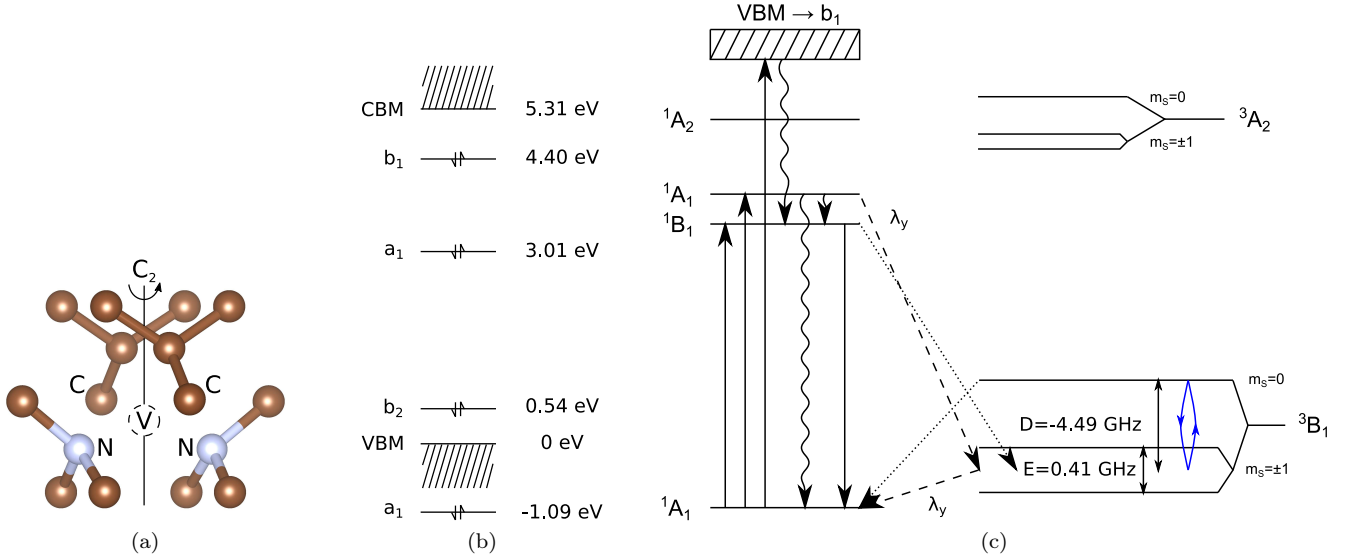


FIG. 1. (a) Geometry of N₂V defect in diamond. (b) Representation of defect levels of N₂V⁽²⁻⁾ with closed-shell orbitals relative to the valence band maximum (VBM). (c) Analysis of ODMR contrast of the neutral N₂V. Straight line illustrates radiative decay, dashed and dotted lines represent ISC with first order and second-order spin-orbit couplings (λ), respectively. Curved lines and blue arrows indicate phonon and microwave transition, respectively. The calculated zero field splitting parameters are given for ³B₁ state at 0 K temperature.

Hamiltonian. Our novel method can be useful in the study of other related quantum bits with highly correlated electronic states.

By using HSE06 we found in an earlier study[25] that the $(+|0)$ and $(0|-)$ charge transition levels of N₂V defect are at $E_C - 4.8$ eV and $E_V + 3.3$ eV, respectively, where E_C and E_V is the conduction and valence band edge, respectively. This explains the stability of its neutral charge state at various doping concentrations. Furthermore, its H13 absorption band can be associated with the transitions from the valence band to the empty in-gap defect level of the neutral defect. The method to calculate the lower energy states and electronic structure is given in the next paragraphs in this Letter. Our basic results are summarized in Fig. 1 that shows the optically induced electron spinpolarization process. We find two optically active excited states (¹B₁ and ¹A₁ with small energy gap) and an optically forbidden dark state (¹A₂). After the excitation to the phonon side band of the optically allowed singlet excited states, it can relax to the vibronic ground state of ¹B₁, and then back to the ¹A₁ electronic ground state with emitting a photon. Alternatively, intersystem crossing (ISC) from ¹B₁ to ³B₁ may take place too as a second order process, where mixing of the excited ¹B₁ and ¹A₁ states caused by B₁-type phonons makes the intersystem crossing feasible via spin-orbit interaction. At elevated temperatures, the ¹A₁ excited state may be thermally occupied (experimental gap is 16 meV in Ref. 7) and then a first order ISC to ³B₁ can occur. This is a *spin selective* transition to $m_S = \pm 1$ as

only λ_y of B₁ symmetry can couple these states, where λ_y is the y -component of the spin-orbit coupling. We note that the spin sublevels of the triplet split even at zero magnetic field that is caused by the electron spin - electron spin dipolar interaction (zero-field splitting) because of the low-symmetry crystal field. Thus, the spin selective ISC will indeed populate only the $m_S = \pm 1$ states. From this metastable triplet, an ISC can occur to the singlet ground state. Again, the transition from the triplet $m_S = \pm 1$ and $m_S = 0$ substates to the singlet ¹A₁ ground state is a first order and a second order process, respectively, because of the selection rules. The singlet-triplet ISC is expected to be significantly slower than the rate of the radiative decay, because the large gap between the excited state singlet and the metastable triplet according to our *ab initio* result. This is in contrast to the interpretation of an experiment [11], that we will discuss below. This *ab initio* result may explain the large quantum yield of the defect. In the optical cycle, ODMR contrast can be achieved by microwave excitation, owing to the lifetime differences of first and second order transitions from the different triplet substates to the singlet ground state. The system shows characteristics that makes it a promising candidate for quantum memory applications. Electron spin polarization can be achieved in the ODMR cycle by populating the $m_S = \pm 1$ sublevel of the metastable triplet. Spin polarization transfer between electron and nearby nuclear spins can be realized by LAC[14], for instance, thus initialization and readout of nuclear spin quantum bits are feasible. The ¹⁴N (or

^{15}N nuclei of the defect and ^{13}C nuclei in their vicinity are candidates for quantum memory. The calculated hyperfine constants are listed for these nuclear spins in Ref. 24. After the nuclear spin was set the electron will naturally decay to the singlet ground state that does not decohere the nuclear spin.

Next, we discuss the nature of electronic structure of the neutral N_2V and methods to calculate it properly. The four dangling bonds of the defect under C_{2v} symmetry produces b_2 , a_1 and b_1 Kohn-Sham levels in the gap, in ascending energy order (see Ref. 24), that may be derived from a split t_2 state of the vacancy. In addition, another a_1 forms resonant with the valence band. These states are occupied by six electrons. The highest energy occupied in-gap a_1 state (HOMO) is a stretched C-C bonding state while the lowest energy empty b_1 state (LUMO) is a C-C antibonding state (see the wavefunctions in Ref. 24) [26]. As we will show below, HSE06 DFT calculations cannot describe the various multiplet states of the defect caused by the strong correlation of open-shell orbitals. In the following we will use a Hubbard model Hamiltonian to represent the strongly correlating electrons. We particularly focus on the HOMO a_1 and LUMO b_1 states as active space for the correlated electrons that contribute to the lowest energy excitations.

Our active space with a_1 and b_1 states may be labeled simply a and b , respectively. Then these states may be given as $a = \frac{1}{\sqrt{2}}(A+B)$ and $b = \frac{1}{\sqrt{2}}(A-B)$ where A and B are dangling bonds on the two nearest neighbor carbon atoms. The singlet determinants with A_1 symmetry are $|^1A_{1(g)}\rangle = |a^\uparrow a^\downarrow\rangle$, $|^1A_{1(e)}\rangle = |b^\uparrow b^\downarrow\rangle$, $|^1B_1\rangle = \frac{1}{\sqrt{2}}(|a^\uparrow b^\downarrow\rangle - |a^\downarrow b^\uparrow\rangle)$. The triplet determinants are $|^3B_1\rangle = |a^\uparrow b^\uparrow\rangle; |a^\downarrow b^\downarrow\rangle$ for $m_S = \pm 1$, respectively, and $|^3B_1\rangle = \frac{1}{\sqrt{2}}(|a^\uparrow b^\downarrow\rangle + |a^\downarrow b^\uparrow\rangle)$ for $m_S = 0$. Substituting a and b in the above formulas, the atomic orbital form of the determinants can be obtained. The electronic structure of the neutral N_2V defect can be described by a Hamilton operator derived from configurational interaction with zero differential overlap (ZDO) approximation and Heisenberg spin coupling. This is a Hamiltonian familiar with the Hubbard model[27]

$$\begin{aligned} \hat{H} = & U (\hat{n}_{A^\uparrow} \hat{n}_{A^\downarrow} + \hat{n}_{B^\uparrow} \hat{n}_{B^\downarrow}) \\ & - \frac{t}{4} (\hat{c}_{A^\uparrow}^\dagger \hat{c}_{B^\uparrow} + \hat{c}_{A^\downarrow}^\dagger \hat{c}_{B^\downarrow} + \hat{c}_{B^\uparrow}^\dagger \hat{c}_{A^\uparrow} + \hat{c}_{B^\downarrow}^\dagger \hat{c}_{A^\downarrow}) \\ & + C (\hat{n}_{A^\uparrow} \hat{n}_{B^\uparrow} + \hat{n}_{A^\downarrow} \hat{n}_{B^\downarrow} + \hat{n}_{A^\uparrow} \hat{n}_{B^\downarrow} + \hat{n}_{A^\downarrow} \hat{n}_{B^\uparrow}) \\ & - 2J (\hat{c}_{A^\uparrow}^\dagger \hat{c}_{A^\downarrow} \hat{c}_{B^\downarrow}^\dagger \hat{c}_{B^\uparrow} + \hat{c}_{A^\downarrow}^\dagger \hat{c}_{A^\uparrow} \hat{c}_{B^\uparrow}^\dagger \hat{c}_{B^\downarrow}) \\ & - J (\hat{n}_{A^\uparrow} \hat{n}_{B^\uparrow} + \hat{n}_{A^\downarrow} \hat{n}_{B^\downarrow} - \hat{n}_{A^\downarrow} \hat{n}_{B^\uparrow} - \hat{n}_{A^\uparrow} \hat{n}_{B^\downarrow}) \end{aligned} \quad (1)$$

where the first term is the onsite repulsion, the second is the hopping, the third is the Coulomb repulsion and the last two terms are from the Heisenberg exchange interaction. \hat{n} is the particle number operator while \hat{c}^\dagger and \hat{c} is the creation and annihilation operators, respectively.

TABLE I. HSE06 total energies of considered states of neutral N_2V relative to that of Ψ_1 obtained by fixed orbital calculation from the $\text{N}_2\text{V}^{(2-)}$ basis states using the N_2V^0 optimized geometry.

state	relative energy (eV)
Ψ_1	0.00
Ψ_2	1.01
Ψ_3	2.23
3B_1	-0.05

We use the symmetry adapted basis above to write down the matrix of the Hamilton operator,

$$H = \begin{pmatrix} |^1A_{1(g)}\rangle & |^1A_{1(e)}\rangle & |^1B_1\rangle & |^3B_1\rangle \\ \frac{U-t+C+3J}{2} & \frac{U-C-3J}{2} & & \\ \frac{U-C-3J}{2} & \frac{U+t+C+3J}{2} & & \\ & & U & \\ & & & C-J \end{pmatrix}, \quad (2)$$

where we here neglected the zero-field splitting in the 3B_1 state. In the HSE06 DFT functional calculations the off-diagonal terms are completely neglected, with resulting in Ψ_1 and Ψ_3 states with 1A_1 symmetry. The 1B_1 state is a multideterminant state, and HSE06 DFT cannot calculate the true eigenstate, and as a consequence, the true eigenenergy of the system. Instead, one can calculate

$$E(\Psi_2) = \langle a^\uparrow b^\downarrow | H | a^\uparrow b^\downarrow \rangle = \frac{U+C-J}{2}. \quad (3)$$

Finally, one can calculate the HSE06 DFT total energies for Ψ_1 , Ψ_3 , 3B_1 (corresponding diagonal terms in Eq. 2) and for Ψ_2 (Eq. 3), that provides four equations for the Hubbard Hamiltonian parameters. The HSE06 DFT total energies for these various states can be obtained by ΔSCF calculations [28]. In order to work with a non-correlated basis for ΔSCF energy calculations required in the Hubbard Hamiltonian, we used the basis functions of the closed shell system of the defect $\text{N}_2\text{V}^{(2-)}$ [Fig. 1(b)], calculated in the N_2V^0 ground state geometry.

After diagonalizing Eq. 2, the vertical excitation energies of the $^1A_{1(e)}$, 1B_1 , and 3B_1 can be calculated (see the expressions and results in Ref. 24) that depend on t , $U-C$, and J parameters. By calculating the HSE06 DFT energies for the afore-mentioned states (summarized in Table I), the parameters in the Hubbard Hamiltonian can be calculated *ab initio*, and the resultant values are $t = 2.23$ eV, $U-C = 2.05$ eV, and $J = 0.05$ eV, respectively. The singlet-triplet coupling is minor, and the $U-C$ terms and the hopping term t dominate, $U-C \approx t \approx 2$ eV. A very important finding is that the ratio of the $^1A_{1(g)} \rightarrow ^1B_1$ and $^1A_{1(g)} \rightarrow ^1A_{1(e)}$ excitation energies scales up by $\approx 1 + \sqrt{2}/2 \approx 1.7$ in the Hubbard model with respect to the DFT results. As a consequence, the excitation energies of the two transitions will be closer to each other in the Hubbard model.

Furthermore, these vertical excitation energies increase in the order of eV in the Hubbard model with respect to the Kohn-Sham HSE06 DFT results. The error in the Kohn-Sham DFT HSE06 functional is much larger than the usual 0.1 eV[25]. Our Hubbard model Hamiltonian derivation clearly shows that the 1B_1 state is a particularly highly correlated multiplet which cannot be properly treated by Kohn-Sham hybrid density functionals.

For direct comparison to the experimental ZPL data, one has to calculate the relaxation energy of ions upon excitation. The relaxation energy was roughly estimated by Δ SCF method on Ψ_{1-3} states. We find that the relaxation energy on $^1A_{1(e)}$ state is ≈ 0.6 eV whereas it is ≈ 0.2 eV on 1B_1 state. The relaxation energy on 3B_1 is small, 0.06 eV. The final results are depicted in Fig. 2 that are directly compared to experimental data and Kohn-Sham HSE06 results. Our Hubbard model Hamiltonian with *ab initio* parameters provides significantly improved results over those of Kohn-Sham HSE06 functional. We find that the $^1A_{1(g)} \rightarrow ^1B_1$ ZPL energy is indeed around 2.4 eV, and the $^1A_{1(g)} \rightarrow ^1A_{1(e)}$ ZPL energy is slightly above that. These are the optically allowed transitions. Higher energy singlet and triplet states with $b_2 \rightarrow b_1$ excitation may form with optically forbidden A_2 symmetry. The 1A_2 state cannot absorb light but can play a role in the non-radiative decay when the electron is excited to the H13 band which corresponds to the valence band to b_1 transition (see Fig. 2). The total energy of the 3A_2 could be calculated Δ SCF procedure from $^3B_1 \rightarrow ^3A_2$ excitation energy whereas the total energy of 1A_2 should be slightly higher due to the small singlet-triplet coupling J .

Regarding the triplet energy levels, their energies in the region of 270 – 480 meV below the 1B_1 level were proposed from PL lifetime measurements where they found a delayed luminescence of millisecond lifetime[11] that they associated with a spin-orbit mediated tunneling process[29] from the metastable triplets to the lowest energy singlet excited state with the formula

$$W(T) = \frac{C}{\sqrt{kT^*}} \coth\left(\frac{\hbar\omega}{2kT}\right) \exp\left(-\frac{E_a}{kT^*}\right) \quad (4)$$

$$C = \frac{|C_{sl}|^2 \omega \sqrt{2\pi}}{\sqrt{2E_M}} \quad (5)$$

$$C_{sl} = \frac{\langle s | \hat{H}_{SO} | l \rangle J_{sl}}{E_s - E_l}, \quad (6)$$

with $kT^* = \frac{1}{2}\hbar\omega \coth(\hbar\omega/2kT)$, E_a is the barrier energy between the corresponding states, $\hbar\omega$ dominant phonon frequency, E_M is the relaxation energy between the two states, k is the Boltzmann constant and T is the temperature in Kelvin. C_{sl} is the coupling of states s and l where \hat{H}_{SO} is the spin-orbit coupling operator, J_{sl} is the

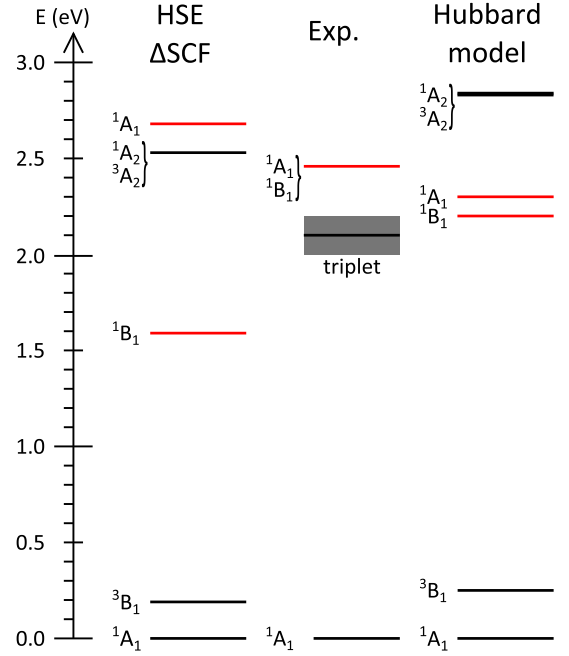


FIG. 2. Excitation energies of the neutral N_2V defect in diamond. States that are very close in energy are enclosed with brackets. The lowest optically allowed excitation energies are highlighted with red. Left panel: Kohn-Sham HSE06 Δ SCF results. Middle panel: experimental zero-phonon-line energies for the singlets (Ref. 7) and the proposed energies of triplets (Ref. 11). Right panel: Hubbard model Hamiltonian results.

electron-phonon coupling. We found that the 3B_1 level is rather far (> 2 eV) from the excited singlet states, thus we estimated its delayed luminescence. As the transition from 3B_1 to 1B_1 is a second order process which should be presumably slow, we calculated the transition to 1A_1 with first order ISC process. The estimated strength of spin-orbit coupling is around 10 GHz and that of the electron-phonon coupling is $0.1 \sqrt{\text{eV}}$, similar to the values in NV center[30, 31]. From our vibrational analysis, calculated with the computationally less expensive PBE functional[32] using PBE optimized geometries, we obtained the average phonon energy of 84 meV weighted by the partial Huang-Rhys factors[33] for the vibrational coupling for this transition. The relaxation energy between 1A_1 and 3B_1 is estimated to be 0.4 eV. With these parameters we obtain a lifetime in the order of 10^6 s at various temperatures. This implies that the observed delayed luminescence is not intrinsic to the defect.

We analyzed the neutral N_2V defect in diamond by means of *ab initio* calculations, and concluded that a quantum memory can be realized by this defect controlled by optical excitation and microwave manipulation. We showed that the electronic structure of this defect is a prototype of highly correlated states that can be treated by our novel method that is a combination of density functional theory and a Hubbard model.

-
- [1] J. E. Field, *The Properties of diamond*. (London: Academic Press, 1976).
- [2] G. Davies and M. F. Hamer, Proceedings of the Royal Society of London. A: Mathematical and Physical Sciences **348**, 285 (1976), <http://rspa.royalsocietypublishing.org/content/348/1653/285.full.pdf>.
- [3] A. Mainwood, Phys. Rev. B **49**, 7934 (1994).
- [4] G. Davies, Journal of Physics C: Solid State Physics **9**, L537 (1976).
- [5] J. Lowther, Journal of Physics and Chemistry of Solids **45**, 127 (1984).
- [6] R. Jones, P. R. Briddon, S. Öberg, and V. J. Torres, in *Defects in Semiconductors 17*, Materials Science Forum, Vol. 143 (Trans Tech Publications, 1993) pp. 45–50.
- [7] G. Davies, M. H. Nazare, and M. F. Hamer, Proceedings of the Royal Society of London A: Mathematical, Physical and Engineering Sciences **351**, 245 (1976), <http://rspa.royalsocietypublishing.org/content/351/1665/245.full.pdf>.
- [8] M. D. Crossfield, G. Davies, A. T. Collins, and E. C. Lightowlers, Journal of Physics C: Solid State Physics **7**, 1909 (1974).
- [9] J.-H. Hsu, W.-D. Su, K.-L. Yang, Y.-K. Tzeng, and H.-C. Chang, Applied Physics Letters **98**, 193116 (2011), <http://dx.doi.org/10.1063/1.3591156>.
- [10] A. T. Collins, Journal of Physics C: Solid State Physics **16**, 6691 (1983).
- [11] E. Pereira and T. Monteiro, Journal of Luminescence **48**, 814 (1991).
- [12] J. A. van Wyk and G. S. Woods, Journal of Physics: Condensed Matter **7**, 5901 (1995).
- [13] A. Gruber, A. Dräbenstedt, C. Tietz, L. Fleury, J. Wrachtrup, and C. von Borczyskowski, Science **276**, 2012 (1997).
- [14] S.-Y. Lee, M. Widmann, T. Rendler, M. W. Doherty, T. M. Babinec, S. Yang, M. Eyer, P. Siyushev, B. J. M. Hausmann, M. Loncar, Z. Bodrog, A. Gali, N. B. Manson, H. Fedder, and J. Wrachtrup, Nat Nano **8**, 487 (2013).
- [15] U. von Barth, Phys. Rev. A **20**, 1693 (1979).
- [16] J. Heyd, G. E. Scuseria, and M. Ernzerhof, The Journal of Chemical Physics **118**, 8207 (2003).
- [17] G. Kresse and J. Hafner, Phys. Rev. B **47**, 558 (1993).
- [18] G. Kresse and J. Furthmüller, Phys. Rev. B **54**, 11169 (1996).
- [19] G. Kresse and J. Furthmüller, Computational Materials Science **6**, 15 (1996).
- [20] J. Paier, M. Marsman, K. Hummer, G. Kresse, I. C. Gerber, and J. G. Ángyán, The Journal of Chemical Physics **124**, 154709 (2006).
- [21] P. E. Blöchl, Phys. Rev. B **50**, 17953 (1994).
- [22] K. Szász, T. Hornos, M. Marsman, and A. Gali, Phys. Rev. B **88**, 075202 (2013).
- [23] V. Ivády, T. Simon, J. R. Maze, I. A. Abrikosov, and A. Gali, Phys. Rev. B **90**, 235205 (2014).
- [24] Supplementary Materials is provided with this manuscript at <http://www.rsc.org>.
- [25] P. Deák, B. Aradi, M. Kaviani, T. Frauenheim, and A. Gali, Phys. Rev. B **89**, 075203 (2014).
- [26] A. S. Zyubin, A. M. Mebel, M. Hayashi, H. C. Chang, and S. H. Lin, The Journal of Physical Chemistry C **113**, 10432 (2009), <http://dx.doi.org/10.1021/jp9012703>.
- [27] J. Hubbard, Proceedings of the Royal Society of London A: Mathematical, Physical and Engineering Sciences **276**, 238 (1963), <http://rspa.royalsocietypublishing.org/content/276/1365/238.full.pdf>.
- [28] A. Gali, E. Janzén, P. Deák, G. Kresse, and E. Kaxiras, Phys. Rev. Lett. **103**, 186404 (2009).
- [29] K. F. Freed and J. Jortner, The Journal of Chemical Physics **52**, 6272 (1970), <http://dx.doi.org/10.1063/1.1672938>.
- [30] A. Batalov, V. Jacques, F. Kaiser, P. Siyushev, P. Neumann, L. J. Rogers, R. L. McMurtrie, N. B. Manson, F. Jelezko, and J. Wrachtrup, Phys. Rev. Lett. **102**, 195506 (2009).
- [31] G. Thiering and A. Gali, submitted (2017).
- [32] J. P. Perdew, K. Burke, and M. Ernzerhof, Phys. Rev. Lett. **77**, 3865 (1996).
- [33] K. Huang and A. Rhys, Proceedings of the Royal Society of London A: Mathematical, Physical and Engineering Sciences **204**, 406 (1950), <http://rspa.royalsocietypublishing.org/content/204/1078/406.full.pdf>.